APPLYING SYMMETRIES DETECTION AT P-BAND POLINSAR DATA

Sofiane Tahraoui[1], Carmine Clemente[2], Luca Pallotta[3], John J. Soraghan[2], and Mounira Ouarzeddine[1]

[1] ***LTIR**, FEI,University of sciences and technologies "USTHB", BP 32 El Alia 16111, Bab Ezzouar, Algeria.*
[2] ***CESIP** group, University of Strathclyde, 16 Richmond St, Glasgow, UK.*
[3] ***CNIT** c/o udr Università degli Studi di Napoli "Federico II " 80125 Napoli, Italy*

ABSTRACT

This paper investigates the potential of synergies between polarimetry and interferometry techniques in SAR data (**PolInSAR**) for the purpose of covariance symmetries detection. The proposed approach will be shown to be able to exploit the peculiar structures of the covariance matrices of PolInSAR images and to discriminate symmetries within the pixel under test. The performance analysis was evaluated using simulated and operational Sensors data and showed a good outcome.

Key words: PolInSAR; Symmetries; Detection; Reflection Symmetry; Rotation Symmetry; Azimuth Symmetry; Cross-Covariance.

1. INTRODUCTION

The polarimetric scattering phenomenon of a medium can be described completely using the covariance matrix [NYKL92]. In general, the medium encountered exhibits symmetric properties, which is detectable through the associated covariance matrix form. However, the backscattered signal from the high-altitude natural targets is always a mixture of responses from elementary scatterers along the vertical positions, particularly in forest areas. This phenomenon does not allow differentiation between symmetry sources. Thus a technique is required that is able to discriminate between the different contributions. The purpose of this paper is to present a new methodology that uses **PolInSAR** technique instead of **PolSAR** [PCMS 1], for the detection of target's symmetries, since it enables the estimation of elevation in each resolution cell. The proposed framework is validated on both simulated and real SAR data demonstrating its effectiveness. The remainder of the paper is organized as follows. Section II introduces the basic concept and describes different symmetries properties. The proposed framework for detecting covariance symmetries in **PolInSAR** is developed in Section III. The performance of the proposed technique applied both on simulated and on real L-band SAR data are presented and discussed in Section IV. Finally, some remarks are given before we conclude the paper.

2. CROSS–COVARIANCE PROPERTIES OF SYMMETRIC TARGET

In monostatic PolInSAR systems, the imaging area is scanned at least twice from slightly different angles. As a result, the system produces one master and slave images and their related scattering matrices. The simpler scenario is represented when only one slave image is generated and is called bi-scanning system yielding to two scattering vectors [CP97], namely $\overrightarrow{k}_m$, and $\overrightarrow{k}_s$, where the subscript m stands for master and s stands for slave:

$$\overrightarrow{k}_m = \frac{1}{\sqrt{2}} \begin{pmatrix} \overbrace{S_{hh_m}}^{\overrightarrow{u}_m} \\ \sqrt{2}S_{hv_m} \\ S_{vv_m} \end{pmatrix} \qquad \overrightarrow{k}_s = \frac{1}{\sqrt{2}} \begin{pmatrix} \overbrace{S_{hh_s}}^{\overrightarrow{u}_s} \\ \sqrt{2}S_{hv_s} \\ S_{vv_s} \end{pmatrix} \quad (1)$$

The subscripts hh, vv, and hv identify the transmitter/receiver polarimetric SAR channels.
The complete scattering phenomenon representing one resolution cell can be described using a (6×6) covariance matrix $\mathbf{C}_6$, formed using the superposition of the scattering vectors (1):

$$\mathbf{C}_6 = \left\langle \begin{bmatrix} \overrightarrow{k}_m \\ \overrightarrow{k}_s \end{bmatrix} \begin{bmatrix} \overrightarrow{k}_m^H & \overrightarrow{k}_s^H \end{bmatrix} \right\rangle = \begin{bmatrix} \mathbf{C}_{11} & \mathbf{C}_{12} \\ \mathbf{C}_{21} & \mathbf{C}_{22} \end{bmatrix}$$

where $\mathbf{C}_{11}$ and $\mathbf{C}_{22}$ are the 3×3 conventional Hermitian polarimetric covariance matrices of each image separately; $\mathbf{C}_{12}$ and/or $\mathbf{C}_{21}$ is the 3×3 cross-covariance matrix that contains not only polarimetric information but also information related to the interferometric phases of different polarisation channels. When the medium exhibits symmetric properties, these polarimetric matrices (i.e $\mathbf{C}_{11}$ or $\mathbf{C}_{22}$), and PolInSAR matrices (i.e $\mathbf{C}_{12}$ and $\mathbf{C}_{21}$), show a particular structure [Mog01]. Moreover, the use of the cross-covariance matrix, enable us to localize in the vertical direction the

detected symmetries. The cross-covariance matrix, in presence of reciprocal medium [LP02, NYKL92] is:

$$\overbrace{\begin{bmatrix} \langle S_{hh_m} S^*_{hh_s} \rangle & \sqrt{2}\langle S_{hh_m} S^*_{hv_s} \rangle & \langle S_{hh_m} S^*_{vv_s} \rangle \\ \sqrt{2}\langle S_{hv_m} S^*_{hh_s} \rangle & 2\langle S_{hv_m} S^*_{hv_s} \rangle & \sqrt{2}\langle S_{hv_m} S^*_{vv_s} \rangle \\ \langle S_{vv_m} S^*_{hh_s} \rangle & \sqrt{2}\langle S_{vv_m} S^*_{hv_s} \rangle & \langle S_{vv_m} S^*_{vv_s} \rangle \end{bmatrix}}^{\mathbf{C}_{12}} \quad (2)$$

Among the vast number of forms that the covariance matrix can exhibit, it is desirable to detect canonical structures related to known properties of symmetry. The phase difference between the master and the slave is caused by the difference in the path of the wave between the two acquisitions.
Hereafter, we review the general cross-covariance matrix (i.e $\mathbf{C}_{12}$ and $\mathbf{C}_{21}$) when symmetry properties are predominant on the target in view. Note that the phase center of the volume scattering will be assumed to be the same for all polarisations. And for analytic purposes, we will assume that:

$$|S_{hh_m}| = |S_{hh_s}| \qquad |S_{vv_m}| = |S_{vv_s}| \quad (3)$$

2.1. Reflection symmetry

The refection symmetry is manifested when the medium exhibits a mirror reflection about the incidence plane along the propagation direction plane and h polarization direction. This leads to the following form of the cross-covariance matrices $\mathbf{C}_{Rf}$ [Mog01]:

$$\mathbf{C}_{Rf} = \begin{bmatrix} \langle S_{hh_m} S^*_{hh_s} \rangle & 0 & \langle S_{hh_m} S^*_{vv_s} \rangle \\ 0 & 2\langle S_{hv_m} S^*_{hv_s} \rangle & 0 \\ \langle S_{vv_m} S^*_{hh_s} \rangle & 0 & \langle S_{vv_m} S^*_{vv_s} \rangle \end{bmatrix} \quad (4)$$

2.2. Rotation symmetry

The rotation symmetry is characterized by a covariance matrix invariance under the rotation around the *line of sight* ($\hat{k}$) by any considered angle [NYKL92]:

$$\overbrace{\begin{bmatrix} \langle S_{hh_m} S^*_{hh_s} \rangle & \sqrt{2}\langle S_{hh_m} S^*_{hv_s} \rangle & \langle S_{hh_m} S^*_{vv_s} \rangle \\ -\sqrt{2}\langle S_{hh_m} S^*_{hv_s} \rangle & 2\langle S_{hv_m} S^*_{hv_s} \rangle & \sqrt{2}\langle S_{hh_m} S^*_{hv_s} \rangle \\ \langle S_{hh_m} S^*_{vv_s} \rangle & -\sqrt{2}\langle S_{hh_m} S^*_{hv_s} \rangle & \langle S_{hh_m} S^*_{hh_s} \rangle \end{bmatrix}}^{\mathbf{C}_{Rt}} \quad (5)$$

with $\langle S_{hh_m} S^*_{vv_s} \rangle = \langle S_{hh_m} S^*_{hh_s} \rangle - 4\langle S_{hv_m} S^*_{hv_s} \rangle$

2.3. Azimuth symmetry

The azimuth symmetry arises as the combination of a rotation with a reflection symmetry. In this case, the medium exhibits mirror reflection symmetry in any plane through the rotation axis. Thus the PolInSAR cross-covariance matrix in this case can be written as:

$$\mathbf{C}_{Az} = \begin{bmatrix} \langle S_{hh_m} S^*_{hh_s} \rangle & 0 & \langle S_{hh_m} S^*_{vv_s} \rangle \\ 0 & 2\langle S_{hv_m} S^*_{hv_s} \rangle & 0 \\ \langle S_{hh_m} S^*_{vv_s} \rangle & 0 & \langle S_{hh_m} S^*_{hh_s} \rangle \end{bmatrix} \quad (6)$$

with $\langle S_{hh_m} S^*_{vv_s} \rangle = \langle S_{hh_m} S^*_{hh_s} \rangle - 4\langle S_{hv_m} S^*_{hv_s} \rangle$

An example of azimuth symmetry that can be observed in vegetated is at low frequencies and normal incidence. Actually, the electromagnetic scattering penetrates through foliage canopy and it is backscattered by the horizontal branches and the vertical trunks, producing the azimuthal symmetry [PMO18].

3. SYMMETRIES DETECTION PROCESS

For each pixel under test, the classification problem at hand can be formulated in terms of the following multiple hypothesis test:

- H_1: No symmetry
- H_2 : Reflection symmetry
- H_3 : Rotation symmetry
- H_4 : Azimuth symmetry

We associate to each pixel to the more dominant symmetry property on the base of the specific structure assumed by its covariance matrix under test. Let consider a complex multivariate normal distribution with zero-mean for N-looks 3-dimensional observable random complex vectors $\overrightarrow{u}_i$ with $i \in \{m, s\}$. Under the assumption that the pixel have circular multivariate Gaussian distribution with zero mean and positifs-definite covariance matrix , the probability density function (**pdf**) of the pixel can be written as [Goo03, LP02]:

$$\mathfrak{f}(\overrightarrow{u}_i \mid \mathbf{C}) = \frac{1}{\pi^{3N} \det(\mathbf{C})^N} \exp\{-tr(\mathbf{C}^{-1}\mathbf{S}_0)\} \quad (7)$$

where det(·) denotes the determinant, $tr(\cdot)$ denotes the trace of the matrix, and $\mathbf{S}_0 = [\overrightarrow{u}_m \overrightarrow{u}_s^H]$. Each one of the four classes (i.e. H_1, H_2, H_3, and H_4) has its specific characteristics. We shall call it, the symmetry class and will be denoted as $\mathbf{C}_{sym}$. The Maximum Likelihood (ML) estimate of $\mathbf{C}_{sym}$ can be obtained as the optimal solution to the optimization problem, i.e.,

$$\min_{\mathbf{C}}[\log(\det(\mathbf{C})) + tr(\mathbf{C}^{-1}\frac{\mathbf{S}_0}{N})] \tag{8}$$

In order to solve the problem and overcome the multiple nested hypotheses, we consider the model order selection **MOS** rules as the Generalized Information Criterion (Bayesian Information Criterion (BIC)), the Bayesian Information Criterion (**BIC**) [SS07], and the Embedded Exponential Family (**EEF**) [Kay01]. This, because we believe this guarantees sufficient accuracy, and that GML approach fails in this context. The general theoretical formulation **BIC**, **GIC** and **EFF** are described next.

4. SELECTORS EVALUATION

Let consider the below matrices, that allows us to remove some redundant information, and simplify the analytical tractability:

$$\mathbf{U} = \begin{bmatrix} 0 & 1 & 0 \\ 1 & 0 & 0 \\ 0 & 0 & 1 \end{bmatrix} \quad , \quad \mathfrak{T} = \begin{bmatrix} \frac{1}{\sqrt{2}} & 0 & \frac{1}{\sqrt{2}} \\ \frac{1}{\sqrt{2}} & 0 & -\frac{1}{\sqrt{2}} \\ 0 & 1 & 0 \end{bmatrix}$$

$$\boldsymbol{\mathcal{V}} = \begin{bmatrix} 0 & 1 & 0 \\ 0 & 0 & j \\ 1 & 0 & 0 \end{bmatrix} \tag{9}$$

$$\mathbf{M}_{Rf} = \mathbf{U}\mathbf{C}_{Rf}\mathbf{U}^H = \begin{bmatrix} \mathfrak{a} & 0 \\ 0 & \mathfrak{C}^{\mathfrak{1}}_{\mathfrak{int}} \end{bmatrix}$$

where

$$\mathfrak{C}^{\mathfrak{1}}_{\mathfrak{int}} = \begin{bmatrix} |S_{hh_m}||S_{hh_m}|e^{j\varphi_{int}} & |S_{hh_m}||S_{vv_m}|e^{j\varphi_{int}} \\ |S_{hh_m}||S_{vv_m}|e^{j\varphi_{int}} & |S_{vv_m}||S_{vv_m}|e^{j\varphi_{int}} \end{bmatrix} \tag{10}$$

and

$$\mathfrak{a} = 2|S_{hv_m}||S_{hv_m}|e^{j\varphi_{int}} \tag{11}$$

Under the assumption (3), $\mathfrak{C}^{\mathfrak{1}}_{\mathfrak{int}}$ is a symmetric matrix, and $\mathfrak{a}$ is a complex number containing the vertical position information.

$$\mathbf{M}_{Rt} = \boldsymbol{\mathcal{V}}\mathfrak{T}\mathbf{C}_{Rt}\mathfrak{T}^H\boldsymbol{\mathcal{V}}^H = \begin{bmatrix} \mathbb{T}^{z}_{\mathfrak{int}} & 0 \\ 0 & \mathfrak{b} \end{bmatrix} \tag{12}$$

where

$$\mathbb{T}_{\mathfrak{int}} = 2e^{j\varphi_{int}} \begin{bmatrix} E_{11} & E_{22} \\ E_{22} & E_{11} \end{bmatrix} \tag{13}$$

where
$E_{11} = |S_{hv_m}||S_{hv_s}|$
$E_{22} = |S_{hh_m}||S_{hv_s}|e^{j(\varphi_{hv}-\pi/2)}$.
Thus, $\mathbb{T}_{\mathfrak{int}}$ is a centro-symmetric matrix[1] and $\mathfrak{b} = |S_{hh_m}|(|S_{hh_s}| + |S_{vv_s}|)e^{j\varphi_{int}}$ is a complex number.

$$\mathbf{M}_{Az} = \mathfrak{T}\mathbf{C}_{Az}\mathfrak{T}^H = \begin{bmatrix} \mathfrak{c} & 0 & 0 \\ 0 & \mathfrak{d} & 0 \\ 0 & 0 & \mathfrak{d} \end{bmatrix} \tag{14}$$

where $\mathfrak{c} = |S_{hh_m}|(|S_{hh_s}| + |S_{vv_s}|)e^{j\varphi_{int}}$, and $\mathfrak{d} = 2|S_{hv_m}||S_{hv_s}|e^{j\varphi_{int}}$ are both complex numbers containing the vertical position information.

4.1. The BIC and GIC selector

The rules of the general order selection using **BIC** , and **GIC** proposed in [SS07] can be expressed through the corresponding decision statistics in the following compact form:

$$-2\log\left(f\left(R \mid \hat{\mathbf{C}}^{(n)}\right)\right) + n\eta(n,N) \tag{15}$$

where $\hat{\mathbf{C}}^{(n)}$ is the ML estimate of $\mathbf{C}$ for n parameters, and η represents the penalty term [SS07, BS05]. For each above selector, the associated penalty term is:
- **BIC**: $\eta(n,K) = log(N)$.
- **GIC**: $\eta(n,K) = \rho+1$, with ρ as an integer number greater than or equal to 2.

Hence, for each of the four aforementioned hypotheses, the decision statistic becomes [TCP+07]:

H_1**:**

$$2N\log[\det(\mathbf{S})] + 6N + 6N\log\pi + 9\eta$$

where $\hat{\mathbf{C}}_{sym} = \mathbf{S}$

H_2**:**

$$2N\log[\det(\bar{\mathbf{S}}_{1,1})] + 2N\log(\bar{\mathbf{S}}_{3,3}) + 6N + 6N\log\pi + 5\eta$$

where $\hat{\mathbf{C}}_{sym} = \mathbf{U}^H \begin{bmatrix} \bar{\mathbf{S}}_{1,1} & 0 \\ 0 & \bar{\mathbf{S}}_{3,3} \end{bmatrix} \mathbf{U}$

and $\bar{\mathbf{S}} = \mathbf{U} \begin{bmatrix} \bar{\mathbf{S}}_{1,1} & \bar{\mathbf{S}}_{1,3} \\ \bar{\mathbf{S}}_{3,1} & \bar{\mathbf{S}}_{3,3} \end{bmatrix} \mathbf{U}^H$

[1] A centrosymmetric matrix is a matrix which is symmetric about its center. In particular, in this case, when its entries satisfy $\mathbb{T}_{\mathfrak{int}} = J\mathbb{T}_{\mathfrak{int}}J$, with J an $n \times n$ permutation matrix with ones on the cross diagonal (bottom left to top right) and zeros elsewhere.

H_3:

$$2N\log\left[\det\left(\frac{(\widetilde{\mathbf{S}}_{2,2}+\mathbf{J}\widetilde{\mathbf{S}}_{2,2}^{T}\mathbf{J})}{2}\right)\right]+2N\log\bar{\mathbf{S}}_{1,1}$$
$$+6N+2N\log 2+6N\log\pi+3\eta$$

where

$$\hat{\mathbf{C}}_{sym}=\mathfrak{T}^{H}\boldsymbol{\mathcal{V}}^{H}\begin{bmatrix}\frac{1}{2}(\widetilde{\mathbf{S}}_{1,1}+J\widetilde{\mathbf{S}}_{1,1}J) & 0\\ 0 & \widetilde{\mathbf{S}}_{2,2}\end{bmatrix}\boldsymbol{\mathcal{V}}\mathfrak{T}$$

and $\quad\widetilde{\mathbf{S}}=\boldsymbol{\mathcal{V}}\mathfrak{T}\mathbf{S}\mathfrak{T}^{H}\boldsymbol{\mathcal{V}}^{H}=\begin{bmatrix}\widetilde{\mathbf{S}}_{1,1} & \widetilde{\mathbf{S}}_{1,2}\\ \widetilde{\mathbf{S}}_{2,1} & \widetilde{\mathbf{S}}_{2,2}\end{bmatrix}$

H_4:

$$2N\log(\hat{\mathbf{S}}_{1,1})+4N\log\left(\frac{\hat{\mathbf{S}}_{2,2}+\hat{\mathbf{S}}_{3,3}}{2}\right)+6N$$
$$+2N\log(2)+6N\log\pi+2\eta$$

where $\breve{\mathbf{S}}=\mathfrak{T}\mathbf{S}\mathfrak{T}^{H}$, and $\breve{\mathbf{S}}_{1,1}$, $\breve{\mathbf{S}}_{2,2}$, and $\breve{\mathbf{S}}_{3,3}$ are its diagonals entries.

4.2. The EEF selector

The **EEF** approach, is one novel pdf construction method; its general formulation is:

$$\mathrm{EEF}(i)=\left\{l_{G_i}(\overrightarrow{u}_i)-n(i)\left[\log\left(\frac{l_{G_i}(\overrightarrow{u}_i)}{n(i)}\right)+1\right]\right\}\times U\left(\frac{l_{G_i}(\overrightarrow{u}_i)}{n(i)}+1\right) \quad (16)$$

where

$$l_{G_i}(\overrightarrow{u}_i)=2\log\left[\frac{f(\overrightarrow{u}_i;\hat{\Omega}_m^{(n(i))})}{f(\overrightarrow{u}_i;\hat{\Omega}_m^{(0)})}\right],\quad i=1,2,3,4,$$

with $U(\cdot)$ the Heaviside step function, and for each of the four aforementioned hypotheses, $n(i)$ represents the associated number of unknown parameters, and under the hypothesis that $\hat{\Omega}_m^{(0)}$ is defined as n-dimensional identity matrix, i.e., $\hat{\Omega}_m^{(0)}=\mathbf{I}_n$, $l_{G_i}(\overrightarrow{u}_i)$ becomes [PCMS 1]:

H_1:

$$l_{G_1}(\overrightarrow{u}_i)=-2N\log[\det(\mathbf{S})]-6N+2tr(\mathbf{S}_0)$$

H_2:

$$l_{G_2}(\overrightarrow{u}_i)=-2N\log(\bar{\mathbf{S}}_{1,1})-2N\log[\det(\bar{\mathbf{S}}_{3,3})]$$
$$-6N+2tr(\mathbf{S}_0)$$

H_3:

$$l_{G_3}(\overrightarrow{u}_i)=-2N\log(\bar{\mathbf{S}}_{2,2})$$
$$-2N\log\left[\det\left(\frac{1}{2}(\widetilde{\mathbf{S}}_{1,1}+J\widetilde{\mathbf{S}}_{1,1}^{T}J)\right)\right]$$
$$-6N-2N\log(2)+2tr(\mathbf{S}_0)$$

H_4:

$$l_{G_4}(\overrightarrow{u}_i)=-2N\log(\hat{\mathbf{S}}_{1,1})-2N\log\left(\frac{\hat{\mathbf{S}}_{2,2}+\hat{\mathbf{S}}_{3,3}^{*}}{2}\right)$$
$$-2N\log\left(\frac{\hat{\mathbf{S}}_{2,2}^{*}+\hat{\mathbf{S}}_{3,3}}{2}\right)-6N-2N\log(2)+2tr(\mathbf{S}_0)$$

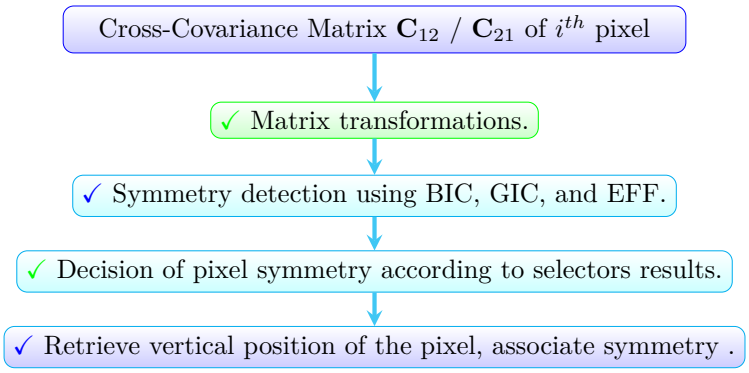

Figure 1: Overall pipeline of PolInSAR Covariance Symmetries detection.

Here we should mention that in the framework at hand, we combines the above three approaches and make a joint decision which give more reliable decision. Figure (1) summarizes the overall pipeline. The input consists of a PolInSAR cross-covariance matrix dataset (i.e $\mathbf{C}_{12}$ or $\mathbf{C}_{21}$). Then we perform a particular transformation for each of the symmetries detection. Then, we apply the **MOS** for detecting the pertinent symmetry. Thereafter, we use the interferometric information to retrieve the associated phase center for the i^{th} resolution cell.

5. P-BAND DATA SYMMETRIES DETECTION

In this part we attempted to validate the PolInSAR covariance detection algorithm at P-band and compared it to the previousely validated one at L-band in [TCP+07]. To this aim we have used the **BiosSAR-II** fully polarimetric at **P** and **L** bands dataset, the selected region is located at $64°14'2.72''N$ Latitude, and $19°47'52.47''E$ Longitude (location indicated by green map-marker in Figure 3). Precisely, the same area has been previously selected for the symmetries detection at L-band in [TCP+07]. Almost all the parts of the zone is forested. The objective is to use the cross-covariance matrix to detect symmetries and its related height.

As shown in Figure 3, the detected symmetries approximately differs for many regions between the two frequencies. The difference in the detected symmetries is due principally to the behavior of EM wave-target interaction, which may change significantly from P-band to L-band. This is caused by two main reasons: a) the penetration depth that plays a key role, because the electromagnetic scattering interaction occurs at different layers from L to P band, meeting different scatterers; b) the sensitivity of EM wave from frequency to another thereby causing the appearance and the disappearance of structure details. In other word, structures with small sizes can not be "seen" (i.e detected) by larger EM wavelengths. On another side the L-band image is acquired with 12 m baseline length, whereas the P-

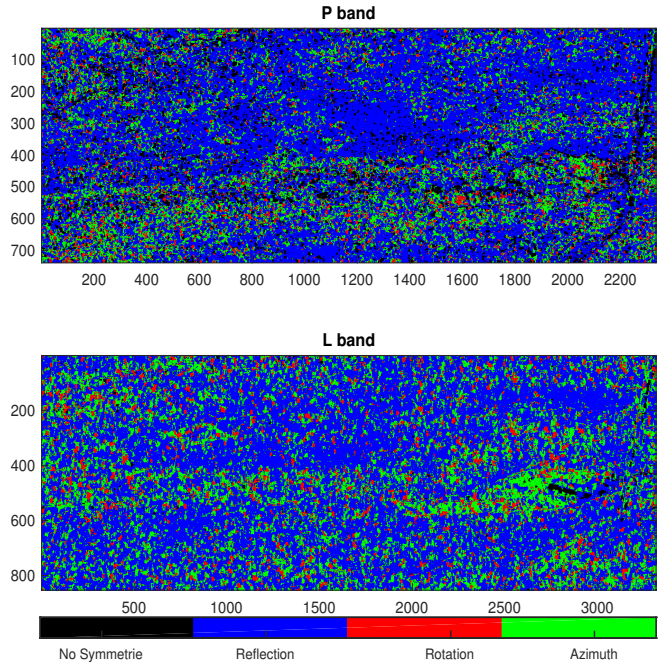

Figure 2: symmetries index associated to the four hypothesis performed using the cross covariance matrix (H_1: no symmetry with black, H_2: reflection symmetry with blue, H_3: rotation symmetry with red, and H_4: azimuth symmetry with green color).

band is acquired with 16 m. The change in baseline length induce changes in viewing angles, which may cause distortion in scatterer perception by sensor, thus, the reflected symmetries is not the same. However, in the case where the scatterer size is larger then the two wavelengths scales, the scatterer form is perceived identically at both frequencies bands, thus, the scatterer still exhibit the same symmetries. This mean that some symmetries form could be detected inside same wavelength scale, whereas some others symmetries are not. For a better visual comparison, Figure 3 shows the resulting detected symmetries from the three estimators *i.e* **BIC**, **GIC**, and **EEF**, as well as their associated vertical positions performed using DEM differencing, carried out along the horizontal blue line. Only PolInSAR phase difference map, scaled from 0 m to 160 m, from 16 m baseline at P band are superimposed on the top (Figure 3). In order to repair detected corresponding symmetry between L and P images for same pixel, the vertical arrows are labeled by numbers . Each of arrow's color indicate specific symmetry (i.e. Black: no symmetries, Blue: reflection symmetries, Red: rotation symmetries, Green: azimuth symmetries). Regardless of compressed form of the profil at L band compared to P band, one may notice clearly by following the labeled arrows the corresponded detected symmetries from image to another. This means that even if we change the frequency band from L to P, some form still depict same symmetries. This fact give evidence to the robustness of the proposed algorithm proposed in [PCMS 1, TCP+07], and make it a trustful algorithm.

6. CONCLUSION

In this paper, the validation of the formulation of detecting covariance symmetries within PolInSAR data has been achieved at P-band. The procedure considers a joint decision according to three selectors namely **BIC**, **GIC**, and **EFF**, in order to deal with the multiple hypothesis testing problem.
The pattern of symmetries at P band has been shown to be different approximatively to L band in some region, which mean that some symmetries form could be detectable at same wavelength scale, whereas some others symmetries are not. Since that the resonant structures of the target interact with the incident electromagnetic field at the wavelength scale, The size of the scatterer relative the wavelength, is of vital importance in details detection. Structures with small sizes can not be detected (i.e "seen") by larger EM wavelengths. Thus, the combination of the detection at the two band could be very interesting. This can help to make appearance of symmetries in one frequency band that are not detectable in the other.
The results was very encouraging, and have opened a promising field of future applications, for example it could be interesting to detect symmetries at multi SAR-frequency (Tomo-symmetries detection) such as in tomographies.

ACKNOWLEDGMENT

The authors would like to thank the BioSAR team and European Space Agency for the data provision.

REFERENCES

[BS05] Kurt Bryan and Yosi Shibberu. Penalty functions and constrained optimization. *Dept. of Mathematics, Rose-Hulman Institute of Technology.*, 2005.

[CP97] S. R. Cloude and K. P. Papathanssiou. Polarimetric optimisation in radar interferometry. *Electronics Letters, June 1997, Vol. 33, No. 13*, pages 1176–1178, 1997.

[Goo03] N. R. Goodman. Statistical analysis based on a certain multivariate complex gaussian distribution (an introduction). *Ann. Math. Statist.*, 34(1):152–177, 1963-03.

[Kay01] S. Kay. Exponentially embedded families - new approaches to model order estimation. *IEEE Transactions on Aerospace and Electronic Systems*, 41(1):333–345, 2005-01.

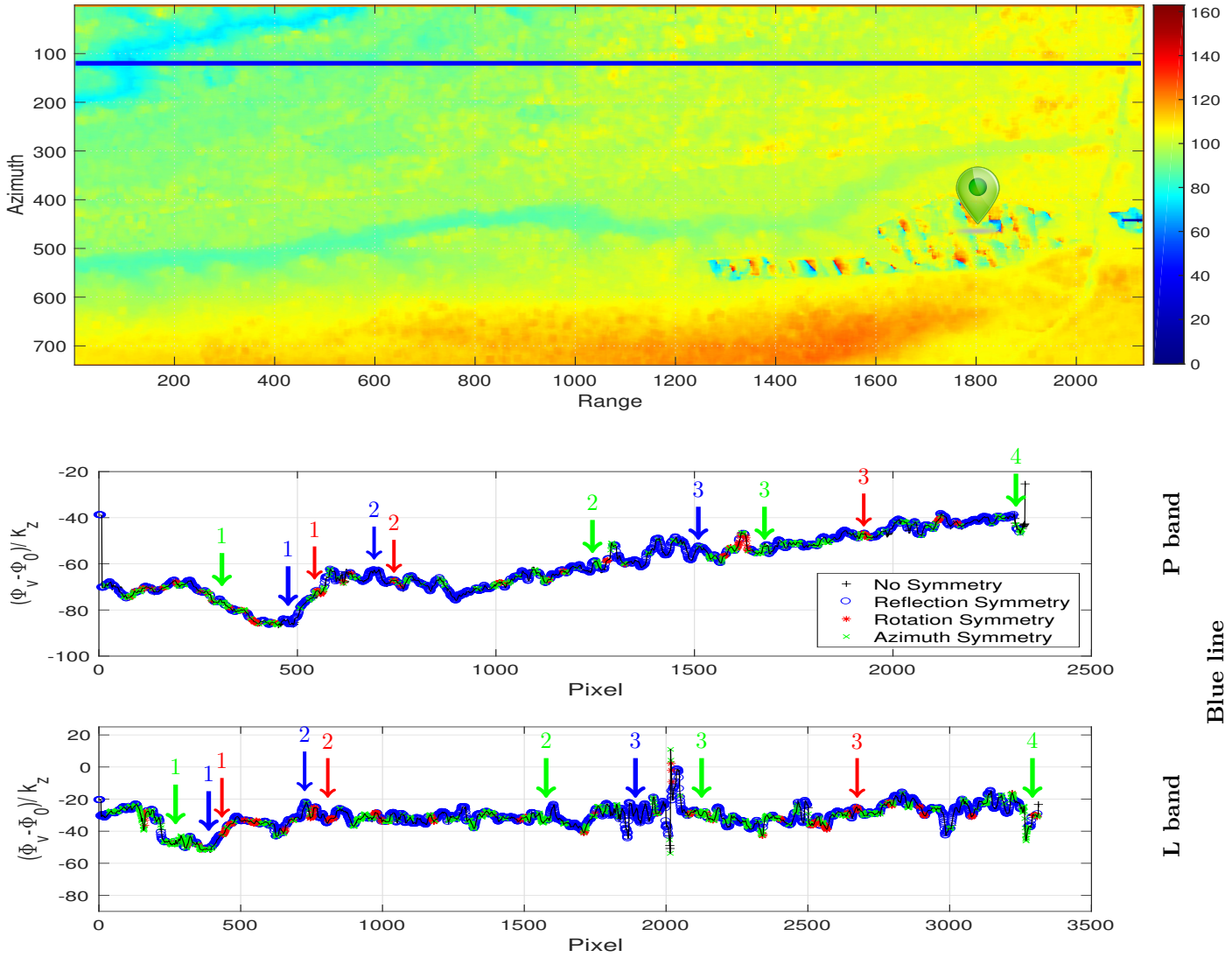

Figure 3: The zone of test from **BiosSAR-II** dataset, (Top) Phase difference images. The two graphs correspond to the estimated horizontal phase profile, carried out along the blue lines, and detected symmetries resulting from BIC, GIC and EEF at P and L bands.

[LP02] Jong-Sen Lee and Eric Pottier. *Polarimetric Radar Imaging: From Basics to Applications*. CRC Press, 1 edition edition, 2009-02-02.

[Mog01] M. Moghaddam. Effect of medium symmetries on limiting the number of parameters estimated with polarimetric SAR interferometry. *Journal of Electromagnetic Waves & Applications*, 1999-01-01.

[NYKL92] S. V. Nghiem, S. H. Yueh, R. Kwok, and F. K. Li. Symmetry properties in polarimetric remote sensing. *Radio Science*, 27(5):693–711, 1992.

[PCMS 1] L. Pallotta, C. Clemente, A. De Maio, and J. J. Soraghan. Detecting covariance symmetries in polarimetric SAR images. *IEEE Transactions on Geoscience and Remote Sensing*, 55(1):80–95, 2017-1.

[PMO18] L. Pallotta, A. De Maio, and D. Orlando. A robust framework for covariance classification in heterogeneous polarimetric SAR images and its application to l-band data. *IEEE Transactions on Geoscience and Remote Sensing*, pages 1–16, 2018.

[SS07] P. Stoica and Y. Selen. Model-order selection: a review of information criterion rules. *IEEE Signal Processing Magazine*, 21(4):36–47, 2004-07.

[TCP+07] Sofiane Tahraoui, Carmine Clemente, Luca Pallotta, John Soraghan, and Mounira Ouarzeddine. Covariance symmetries detection in PolInSAR data. *IEEE Trans TGRS*, PP(7), 2018-07.